Peculiarities of the structural and optical properties of rare-earth-doped phosphate glasses for temperature sensing applications

M. Elisa[1], S.-M. Iordache[1*], A.-M. Iordache[1], I. C. Vasiliu[1], C. E. A. Grigorescu[1], B. A. Sava[2], L. Boroica[2], A. V. Filip[2], M. C. Dinca[2], C. Bartha[3], N. de Acha[4], C. Elosua Aguado[4,5]

[1]Optospintronics Department, National Institute of R & D for Optoelectronics-INOE 2000, 409 Atomistilor Str., 077125, Magurele, Jud. Ilfov, Romania; astatin18@yahoo.com; *istefanmarian@yahoo.com; anaducu@3nanosae.org; icvasiliu@inoe.ro; krisis812@yahoo.co.uk;
[2]Lasers Department, National Institute for Laser, Plasma and Radiation Physics, 409 Atomistilor Str, 077125 Magurele, Jud. Ilfov, Romania; savabogdanalexandru@yahoo.com; lucica_boroica@yahoo.com; ana_filip@ymail.com; catalin69@live.com;
[3]Magnetism and Superconductivity Laboratory, National Institute of Materials Physics, 405 A Atomistilor Str, 077125 Magurele, Jud. Ilfov, Romania, cristinavals@yahoo.com;
[4]Department of Electrical, Electronic and Communications Engineering, Public University of Navarra, E-31006 Pamplona, Spain; nerea.deacha@unavarra.es; cesar.elosua@unavarra.es;
[5]Institute of Smart Cities (ISC), Public University of Navarra, E-31006 Pamplona, Spain cesar.elosua@unavarra.es;
*Corresponding author

Abstract
Eu, Er, Yb-Er, and Dy-doped phosphate glasses were prepared by a wet-route processing of chemical precursors followed by melt-quenching and annealing. XRD measurements highlighted the amorphous nature of the investigated glasses. UV-Vis absorption spectra revealed peaks specific to f-f electronic transitions of the doping ions whereas FTIR and Raman spectroscopy proved the vitreous network forming role of phosphorous pentoxide. Luminescence spectra in the Vis domain, at RT, showed emission bands characteristic to the ion transitions from the excited states to the ground state. The luminescence spectra collected in the ~(25--160^{o}C) range exhibited a decrease of the emission intensity with temperature rise. In the case of Eu and Dy-doped glasses no significant changes were noticed by comparison with Er and, respectively, Yb-Er-doped glass where a significant change of the emission intensity is observed. The change of the emission characteristics upon temperature rise recommends Er and Yb-Er-doped glasses as - promising candidates for sensing devices.

Keywords: rare-earth ions, phosphate glass, optical absorption, Fourier Transform Infrared spectroscopy, Raman spectroscopy, photoluminescence

1. Introduction

Recently, Eu_2O_3-doped glasses and glass ceramics were investigated for orange and red emission devices. Rare earth-doped transparent glass ceramics have lately appealed extensive attention due to their outstanding properties for laser and optoelectronic device applications [1,2]. Glass ceramics are useful composite materials that gather the significant optical properties of the nano-crystalline phase and the remarkable mechanical properties as well as chemical stability of the glass phase [3]. Thus, Eu-doped calcium aluminosilicate glass and glass-ceramics have been synthesized and 532 nm excitation revealed peaks in the 570–750 nm range attributed to $^5D_0 \rightarrow {}^7F_J$ (J=0–4) transitions of Eu^{3+}. The broad band emission due to $4f^6 5\,d^1 \rightarrow 4f^7$ for 473 nm excitation, showed that Eu^{2+} is incorporated into the crystalline phases after reduction of Eu^{3+} during annealing [4]. Eu^{3+}-doped bismuth borosilicate glasses were synthesized by the melt quenching technique. Varying Eu_2O_3 concentration from 0 to 5 mol. %, the emission spectra revealed that Eu^{3+}-doped glasses present the strongest emission at 613 nm ($^5D_0 \rightarrow {}^7F_2$) wavelength when excited with 465 nm, thus making these glasses promising materials for reddish orange emission devices [5]. Luminescence emissions of 1 mol. % Eu_2O_3 embedded in sodium lead phosphate glass matrix have been reported. Upon 393 nm excitation, seven emission bands are revealed: $^5D_1 \rightarrow {}^7F_1$ (535 nm), $^5D_1 \rightarrow {}^7F_2$ (554 nm), $^5D_0 \rightarrow {}^7F_0$ (579 nm), $^5D_0 \rightarrow {}^7F_1$ (592 nm), $^5D_0 \rightarrow {}^7F_2$ (612 nm), $^5D_0 \rightarrow {}^7F_3$ (653 nm) and $^5D_0 \rightarrow {}^7F_4$ (700 nm) respectively. The

most intense one is that from 612 nm, being highly enhanced in lead sodium phosphate glass matrix in comparison to other host matrices reported [6].

The white light emission properties of Dy^{3+} doped glasses and glass ceramics have been lately reported. The emission spectrum of Dy^{3+} doped ZBAN (zirconium-barium-aluminum-sodium) fluoride glasses excited by ultraviolet light at 350 nm shows two strong emission peaks (480 and 575 nm) and one weak emission peak at 660 nm that belongs to $^4F_{9/2}\rightarrow{}^6H_{15/2}$, $^4F_{9/2}\rightarrow{}^6H_{13/2}$, $^4F_{9/2}\rightarrow{}^6H_{11/2}$ transitions, respectively [7]. Recently, bismuth-tellurium-dysprosium-boron silicate glasses (SiBBiTe) have been reported as adequate for WLEDs applications. Two intense bands of luminescence were found at 480 and 575 nm, which correspond to the $^4F_{9/2}\rightarrow{}^6H_{15/2}$ and $^4F_{9/2}\rightarrow{}^6H_{13/2}$ transitions, respectively, and one lower intensity band at 664 nm corresponding to the transition $^4F_{9/2}\rightarrow{}^6H_{11/2}$ [8]. Researchers have found that in Dy^{3+} doped NaO-BaO-Bi_2O_3-SiO_2 glass system the band from 385 nm exhibited the highest absorption in the visible light, while the strongest emission band is centered at 575 nm. Increasing the concentration of Dy^{3+} to 1.5 mol. % leads to two other emission bands 482 nm and 662 nm [9]. Other authors have prepared and characterized single doped (Dy^{3+}) and co-doped (Dy^{3+}/Eu^{3+})-doped potassium-zinc-aluminum-dysprosium phosphate glasses for white luminescence applications. Dy-doped glasses exhibit blue, green and red emission when excited by 350 nm. Luminescence spectra of co-doped Dy^{3+}/Eu^{3+} glasses at different excitation wavelengths (364, 383, 394 and 463 nm) show six emission bands at 483, 575, 593, 615, 662 and 700 nm. The bands at 483 and 575 nm are ascribed to the transitions $^4F_{9/2}\rightarrow{}^6H_{15/2}$ and, respectively, $^4F_{9/2}\rightarrow{}^6H_{13/2}$ due to the Dy^{3+} ion and the rest of the bands are ascribed to the transitions $^5D_0\rightarrow{}^7F_1$, $^5D_0\rightarrow{}^7F_2$, $^5D_0\rightarrow{}^7F_3$ and $^5D_0\rightarrow{}^7F_4$, respectively, due to Eu^{3+} ion [10].

Much work was done on the near infrared (NIR) luminescent properties of Er^{3+}-doped glass matrices, which includes chalcohalide glasses [11,12], tellurite glasses [13,14], germanate glasses [15], and borate glasses [16]. Most works found that near-infrared (NIR) luminescence appears at about 1525 nm under 808 nm excitation with an increase in the intensity of the luminescence following an equal increase of Er dopant up to 2 mol. % [17]. For Er-doped lithium-bismuth-boron-phosphate glasses the NIR emission spectra measured by 980 nm excitation is found to be placed at 1532 nm for the $^4I_{13/2}\rightarrow{}^4I_{15/2}$ transition, which demonstrates that the investigated oxide systems are promising candidates for the broadband amplifiers [18]. Other studies, such as Er^{3+}-doped cadmium-vanadium-phosphate glass samples showed that upon 980 nm diode laser excitation, a near infrared emission is observed, showing a broad band extending from 1440 to 1650 nm, attributed to the Er^{3+}: $^4I_{13/2}\rightarrow{}^4I_{15/2}$ transition, the highest intensity being noticed for 2.5 mol. % Er^{3+} concentration. For higher Er^{3+} concentrations, the emission intensities were progressively reduced due to the non-radiative and cross relaxation processes highlighting a dipole-dipole electric interaction [19].

Other types of doped glasses are promising candidates for application in NIR-optical amplifiers. Thus, Li et al. prepared transparent glass ceramics containing nano-crystalline Er, YbEr-doped $Bi_2ZnB_2O_7$ by high-temperature melting. Yb^{3+} ions improved the symmetry and the coordination field degree around Er^{3+} as well as the emission efficiency of the glass ceramic material. Under 980 nm excitation (corresponding to the transition $^4I_{13/2}\rightarrow{}^4I_{15/2}$), the samples produced a wide-band fluorescence between 1400-1700 nm [20]. Yb^{3+}/Er^{3+} co-doped lithium phosphate glass ceramics doped with 0.05Er_2O_3-0.25Yb_2O_3 (mol. %) synthesized by annealing of the glass at 600 ºC for 24 h, exhibit a strong infrared emission at 1.53 μm [21]. Potassium-niobium germanate glasses and glass ceramics doped with up to 4 mol. % Er_2O_3 show an amplification of the emission intensities at1.5 μm in glass-ceramics with higher erbium contents compared to the precursor glasses. The devitrification of the glass favors the emission around 1.5 μm in relation to the precursor glass while higher erbium contents (> 2 mol. %) quench this emission. This consideration is important because it influences the performance of these materials as optical amplifiers and NIR laser [22]. The near infrared emission of Er^{3+}-doped, Er^{3+}-Yb^{3+} co-doped and Er^{3+}-Mn^{2+}-Yb^{3+} tri-doped aluminum-barium-lanthanum-titanium silicate glasses and glass ceramics was investigated. The forming of Mn^{2+}–Yb^{3+} dimer and the energy transfer processes Mn^{2+}–Yb^{3+} and Mn^{2+}-Er^{3+} has led to a significantly increased NIR emission of Er^{3+}-doped at ∼1.54 μm [23]. Previous works of the coauthors related to optical and structural properties of rare-earth-doped aluminophosphate glasses were reported in [24-28].

There are various luminescent materials employed as optical thermometers, and most of them are based on the competition of electron population in the thermally coupled states (TCS) of rare-earth (RE) ions or transition metal (TM) ones. Optical studies reveal the fact that the radiative properties of RE ions in glasses strongly depend on the host matrix and can be modified by proper choice of network forming and network modifying ions [29-31]. Nowadays, Dy^{3+} ion doped glasses such as, boro-tellurite, fluorophosphate, oxyfluoroborate, lead tellurofluoroborate, lead silicate and zinc alumino bismuth borate glasses are receiving more attention [29]. Eu^{3+}-doped tellurite glasses embedding $CsPbBr_3$ PQDs (perovskite quantum dots) were successfully prepared by Xiaoyan Li and co. The obtained nanocomposite exhibited excellent temperature sensing performance in the temperature range of 93–383 K [32]. High measurement accuracy and wide measurement temperature range can be achieved with Er^{3+}/Yb^{3+} co-doped transparent glass-ceramics containing $NaZnPO_4$ which has potential application in optical temperature sensor [33]. The thermally coupled up-conversion green emission of Er^{3+} ion can be used for temperature sensing, which suggests that the Er^{3+} and Yb^{3+} co-doped zinc phosphate glass might be qualified candidate for temperature sensing [34]. Yb^{3+}/Er^{3+} co-doped phosphate glasses are an efficient up-conversion material with potential application in optical thermometry [35].

In the present paper, phosphate glasses doped by rare-earth ions were synthesized and structural as well as photoluminescence characterization from room temperature to ~160ºC was performed. The photoluminescence sensitivity of Er^{3+}, Yb^{3+}-Er^{3+}, Eu^{3+} and Dy^{3+}-doped glasses with temperature variation was investigated for sensing device applications.

The originality of the work is related to the application of the non-conventional method of processing reactants in solution that guarantees a high chemical and optical homogeneity of the final doped glasses, as presented in previous papers [25,36,37]. At the same time, the reported investigations sustain new rare-earth-doped alumino-phosphate glass compositions having a high chemical stability [36,37], a reduced crystallization tendency together with interesting optical and structural properties which have been investigated in detail. The dependence of photoluminescence on temperature is the base research direction of the present work highlighting the potential application of these vitreous materials for sensing devices.

2. Materials and Methods

In this study, an un-doped phosphate glass and phosphate glasses doped with Eu^{3+}, Dy^{3+}, $Er^{3+}$and Yb^{3+}-Er^{3+}, respectively, were synthesized by a non-conventional wet route of starting reagents processing followed by melt quenching. The homogenization of the chemical reagents in H_3PO_4 solution, accompanied by continuous mechanical stirring of the starting batch as well as of the glass melt ensures a high optical quality of the final vitreous materials [36-40]. Vitreous and glass ceramics materials synthesized from liquid precursors are also presented in [41]. The nominal molar composition of the synthesized glasses is presented in Table 1.

Table 1. Molar composition of rare-earth-doped phosphate glasses.

Glass code	Molar composition
Etalon	$60LiPO_3$ $30Al(PO_3)_3$ $10\ Ba(PO_3)_2$
Eu	$58LiPO_3$ $29Al(PO_3)_3$ $10\ Ba(PO_3)_2$ $3Eu_2O_3$
Dy	$58LiPO_3$ $29Al(PO_3)_3$ $10\ Ba(PO_3)_2$ $3Dy_2O_3$
Er	$58LiPO_3$ $29Al(PO_3)_3$ $10\ Ba(PO_3)_2$ $3Er_2O_3$
Yb-Er	$58LiPO_3$ $29Al(PO_3)_3$, $10\ Ba(PO_3)_2$ $2.5Yb_2O_3$ $0.5Er_2O_3$

As raw materials the following ultra-grade purity reagents have been used: Li_2CO_3, $BaCO_3$, Al_2O_3, Eu_2O_3, Dy_2O_3, Er_2O_3, Yb_2O_3, and H_3PO_4 solution, concentration 85 %, density 1.71 g/cm^3.

As shown in Table 1, the metaphosphate molar composition of the un-doped glass is similar with that of the base vitreous matrix from REPGs, related to $LiPO_3/Al(PO_3)_3$ ratio and $Ba(PO_3)_2$ content.

X-Ray Diffraction (XRD) patterns were recorded with a Bruker D8 Advance device, (CuKα, λ = 1.54056 Å). The XRD data were acquired at room temperature using a step scan interval of 0.020° and a step time of 10 s. All samples were scanned between 10° and 70° 2 (2θ range).

Optical absorption was investigated in the range 300-1800 nm using a Perkin Elmer Lambda 1050 spectrophotometer with a scan rate of 2 nm/min.

Fourier Transform Infrared (FTIR) spectra were recorded with a Perkin Elmer Spectrophotometer-Spectrum 100 provided with Universal Attenuated Total Reflectance (UATR) accessory, in the range 400–4000 cm^{-1}, 4 cm^{-1} resolution, the number of scans 20 and a measurement error of ±0.1%.

Raman spectra were collected with a LABRAM-HR 800 Horiba Jobin Yvon spectrometer, in the 200–2000 cm^{-1} range, Ar^{+} laser excitation (λ=514.5 nm), laser power at the sample surface 2.33 mW, without attenuation filter, accumulation time 5 sec/point, resolution 1 cm^{-1}.

Photoluminescence emission of rare-earth-doped-phosphate glasses (REPGs) was collected with a Horiba Jobin-Yvon Fluorolog 3 spectrofluorometer in the range 400-700 nm, at room temperature, measurement angles 45º and 60º, respectively. The most intense emission was noticed at 45º for all the REPGs. The luminescence measurements in the range ~(25--160ºC) were done by excitation with a laser diode at 365 nm in the case of Eu and Dy-doped glasses and a laser diode at 980 nm in the case of Er and Yb-Er-doped glasses. 600 µm-core bifurcated optical fibers were used to excite and collect the emission, the measurement fiber and the thermocouple being positioned on the glass surface. An USB2000FLG spectrophotometer was used to measure the emission of Eu and Dy-doped glasses (from 350 nm to 800 nm), while the NIR emission of Er and Yb-Er-doped glasses was acquired with the NIR512 spectrophotometer (from 850 nm to 1700 nm). All the spectra were recorded with Spectra Suite software: the integration time was fixed at 1 s, whereas each measurement consisted of the average of three subsequent acquisitions. Both spectrophotometers, as well as the software were purchased from Ocean Optics.

3. Results and Discussion

The results and discussion will be presented in this work in the series: un-doped glass, followed by Eu, Dy, Er and Yb-Er-doped glasses, as the rare-earth elements are found in the 4f lanthanide periodic table, taking into account the decreasing of the ionic radii and increasing of the ionic mass.

3.1. X-ray Diffraction

In Fig. 1, XRD patterns of the un-doped and RE-doped glasses are presented. It is evidenced an amorphous character of the investigated glasses.

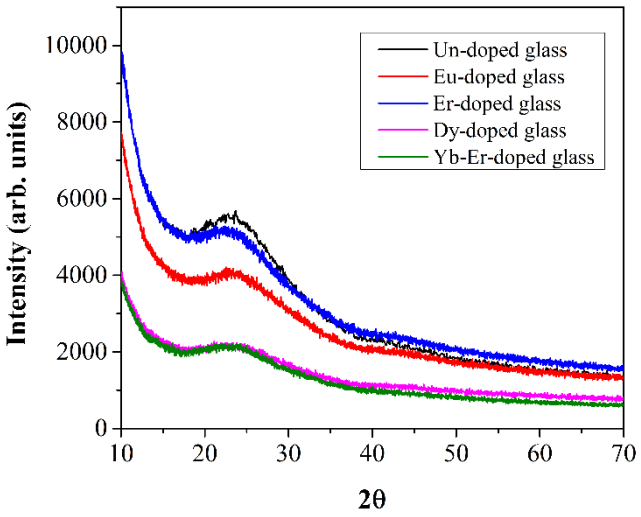

Fig. 1. XRD patterns of un-doped glass, Eu, Er, Dy, and Yb-Er-doped glasses, respectively.

3.2. Optical absorption

Optical absorption of the un-doped and REPGs in the UV-Vis-NIR domain is presented in the Figs. 2a, 2b, 2c and, respectively, 2d. As expected, the un-doped glass does not exhibit absorption bands in the UV-Vis-NIR domain. The absorption spectra of the REPGs reveal peaks specific to f-f electronic transitions of RE doping ions. The glass doped by Eu^{3+} does not exhibit absorption bands located in the NIR domain (Fig.2b) as noticed in the case of Dy^{3+}, Er^{3+} and Yb^{3+}-Er^{3+} -doped glasses (Figs. 2c and 2d). In the visible light region, Eu-doped glass absorb photons at 362, 382, 394, 415, 465, 525 and 532 nm wavelength, corresponding to the transitions $^7F_0 \rightarrow {}^5D_4$, $^7F_0 \rightarrow {}^5G_2$, $^7F_0 \rightarrow {}^5L_6$, $^7F_1 \rightarrow {}^5D_3$, $^7F_0 \rightarrow {}^5D_2$, $^7F_0 \rightarrow {}^5D_1$ and $^7F_1 \rightarrow {}^5D_1$, respectively [35]. The absorption spectrum of Dy-doped glass (Fig.2c) consists in inhomogeneous absorption bands located at 324, 349, 364, 387, 425, 452, 751, 801, 897, 1092, 1270, and 1677 nm, which are assigned to the transitions from the ground state, $^6H_{15/2}$ to the following excited levels: $^6P_{3/2}$, $^6P_{7/2}$, $^6P_{5/2}$ +$^6P_{3/2}$, $^4F_{7/2}$, $^4G_{11/2}$, $^4I_{15/2}$, $^6F_{3/2}$, $^6F_{5/2}$, $^6F_{7/2}$, $^6F_{9/2}$, $^6F_{11/2}$+$^6H_{9/2}$ and $^6H_{11/2}$ [10].

In the case of Er^{3+}-doped glass (Fig.2d), the electronic transitions take place from the ground state $^4I_{15/2}$ to the following energy levels: $^4G_{11/2}$ (364, 378 nm),$^2G_{9/2}$, $^2H_{9/2}$, $^4F_{9/2}$ (406 nm), $^4F_{5/2}$ (450 nm), $^4F_{7/2}$ (488 nm), $^2H_{11/2}$ (520 nm), $^4S_{3/2}$ (544 nm), $^4F_{9/2}$ (650 nm), $^4I_{9/2}$ (798 nm), $^4I_{11/2}$ (978 nm), and $^4I_{13/2}$ (1534 nm) [18, 19]. The only absorption band (978 nm) of Yb^{3+} ions corresponds to the transition $^2F_{7/2} \rightarrow {}^2F_{5/2}$ [43, 44] (Fig.2d).

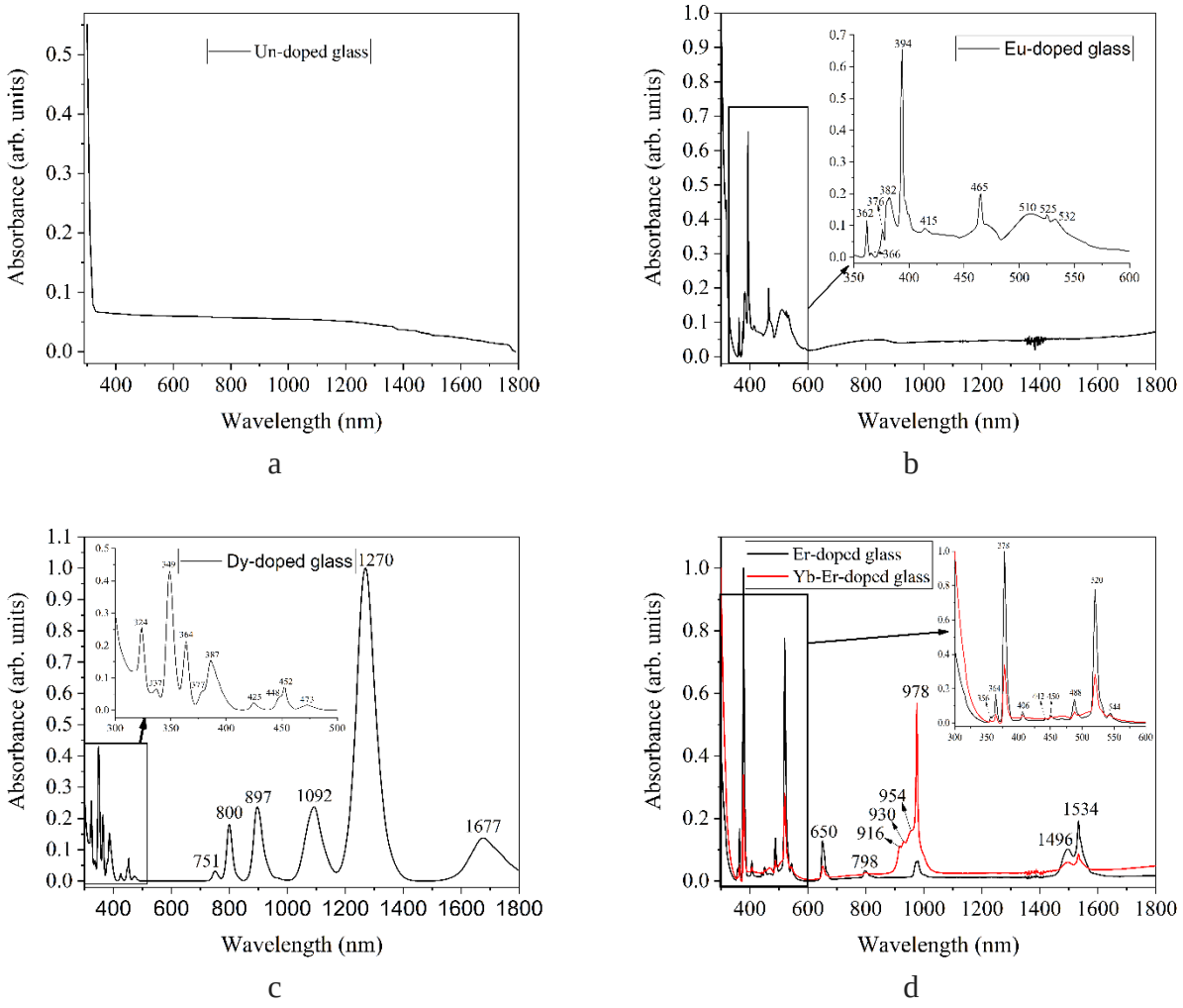

Fig. 2. Optical absorption of a) un-doped; b) Eu; c) Dy and d) Er and Yb-Er doped glasses, respectively.

3.3. Structural analysis

3.3.1. FTIR and Raman spectroscopy

Structural information on the un-doped and REPGs are provided by FTIR and Raman spectroscopy, in the range 450-1500 cm^{-1} and, respectively, 200-1800 cm^{-1}. FTIR and Raman spectra of the un-doped glass are presented in Fig.3a and, respectively, Fig.4a. The deconvolution of the FTIR and Raman bands highlights the bending and stretching vibration modes specific to various phosphate units and bonds. Figs.3b and 4b present FTIR and, respectively, Raman spectra of the un-doped glass compared to the spectra of the REPGs revealing the influence of the dopant ions on the local symmetry. Both FTIR and Raman spectra show peaks characteristic to the phosphate network, emphasizing the network forming role of P_2O_5. Wavenumbers and assignment of both FTIR and Raman bands are given in Table 2.

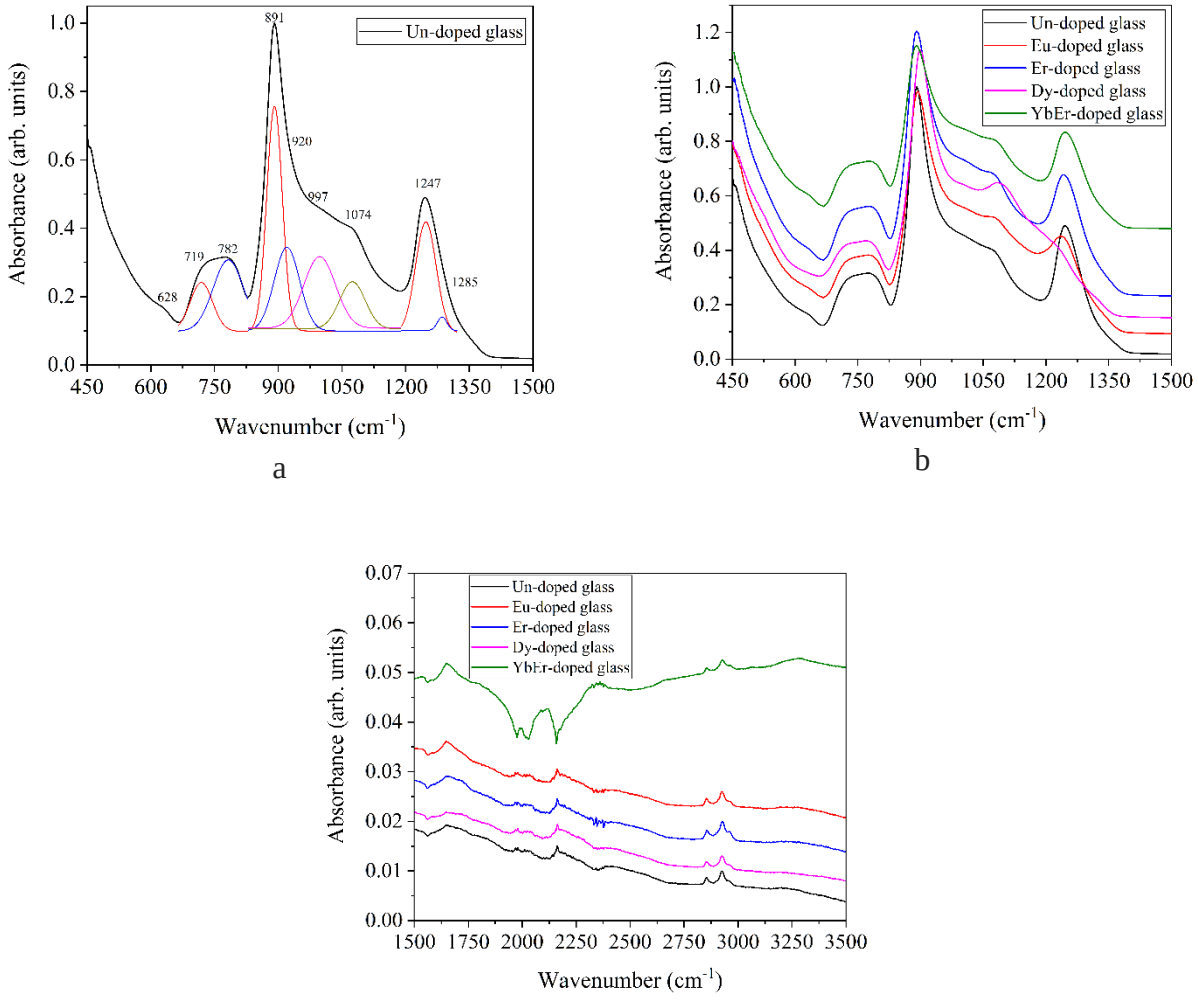

Fig. 3. FTIR spectra of a) un-doped glass in the range 450-1500 cm^{-1}; b) REPGs in the range 450-1500 cm^{-1}; c) REPGs in the range 1500-3500 cm^{-1}.

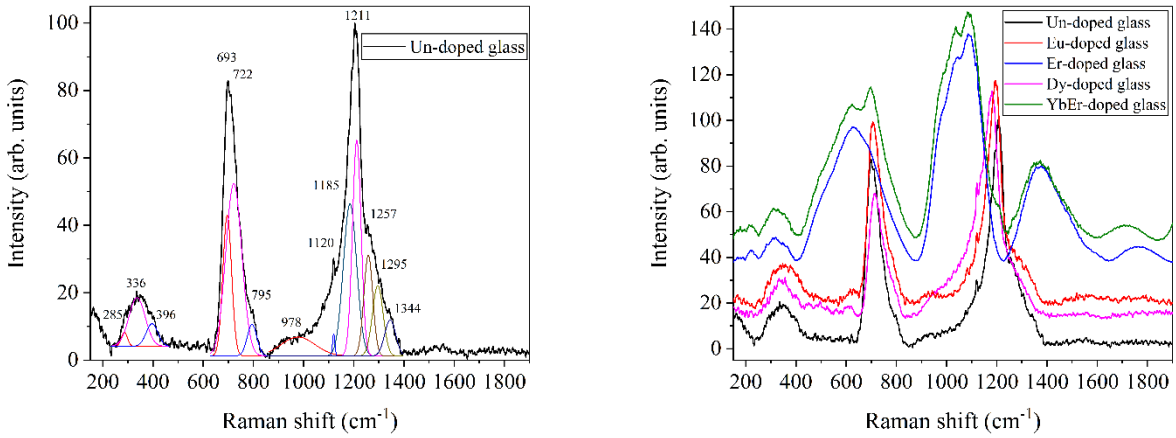

a b

Fig.4. Raman spectra of a) the un-doped glass; b) REPGS.

Table 2. Assignment of FTIR and Raman bands for REPGs

Attributions	FTIR wavenumbers (cm^{-1})					Raman wavenumbers (cm^{-1})				
	Un-doped glass	Eu-doped glass	Dy-doped glass	Er-doped glass	Yb-Er-doped glass	Un-doped glass	Eu-doped glass	Dy-doped glass	Er-doped glass	Yb-Er-doped glass
$\sigma_{(O-P-O)}$ (phosphate polyhedra)	628	628	-	630	630	285; 336; 396;	296; 327; 382; 485; 625	342; 406; 446; 493; 610	220; 281; 316; 347; 369	213; 275; 309; 353; 383
$\nu_{(P-O-P)sym}$ (between Q^1 and Q^2 units)	719	722	720	717	717	693; 722	704; 738	708; 746	487; 600; 630; 689; 751	475; 541; 578; 626; 695; 733
$\nu_{(P-O-P)sym}$ (within Q^2 and Q^1 units)	782	785	778	780	783	795	778; 820	786	-	787
$\nu_{(P-O-P)asym}$	891; 920	893; 958	899; 946	886; 920	884; 919	-	935	945	-	953
$\nu_{(P-O-P)asym}$/ $\nu_{(PO4)sym}$ (Q^0 units)	997	1013	988	988	988	978	-	1013	978; 1015; 1038	987; 1004; 1030
$\nu_{(PO3)^{2-}asym}$	1074	1097	1085	1073	1074	-	-	-	1086	1086
$\nu_{(O-P-O)sym}$/ $\nu_{[(PO3)^{2-}]asym}$	-	-	-	-	-	1120	1102	-	1120	1122
$\nu_{(O-P-O)sym}$ (Q^2 units)	-	-	-	-	-	1185; 1211	1143; 1195	1136; 1182	1135	1138; 1204
$\nu_{(O-P-O)asym}$ (Q^2 units)/	1247	1238	1208	1242	1248	-	-	-	-	-

$\nu_{(P=O)}$ (long phosphate chains)										
$\nu_{(P=O)sym}$	-	-	-	-	-	1257	1253	1233	-	1261
$\nu_{(O-P-O)asym}$	1285	-	-	1340	1338	1295; 1344	1289 1335	1296	1305; 1352	1318; 1369
ν and σ vibration modes and combined vibrations of H-OH bonds	-	-	-	-	-	-	-	-	1380; 1423; 1482; 1537; 1726; 1791; 1845	1406; 1437; 1501; 1707

σ= bending vibration mode
ν=stretching vibration mode

In the following, the discussion of bands assignment will be done comparatively between the un-doped glass and REPGs, taking into consideration the peaks assignment reported in [45-51, ,53,54] for FTIR and, respectively in [48,49,51,55-57] for Raman vibration modes. In the range 220-630 cm^{-1}, bending vibration modes specific to the phosphate polyhedra are noticed. The next range between 640-840 cm^{-1} evidences intense symmetrical stretching vibration modes of P-O-P bonds (bridging oxygen atoms) specific to Q^1 and Q^2 tetrahedra. The Raman peaks specific to these vibration modes are shifted towards lower wavenumbers in the case of Er and Yb-Er-doped glasses possibly due to the modification of the local symmetry, taking into account the increased ionic mass and decreased ionic radii of Er^{3+} and Yb^{3+} ions. The range 830-1200 cm^{-1} for FTIR spectra and 830-1400 cm^{-1} for Raman spectra present intense asymmetrical stretching vibration modes specific to P-O-P bonds and symmetrical stretching vibration modes of $(PO_4)^{3-}$ units from Q^0 tetrahedra (orthophosphate groups). Also, asymmetrical stretching vibration modes of $(PO_3)^{2-}$ units (metaphosphate groups) and symmetrical stretching vibration modes of O-P-O units (non-bridging oxygen atoms) are observed. At higher wavenumbers, symmetrical stretching vibration modes of P=O bonds in long chains, O-P-O asymmetrical stretching vibration mode and bending and stretching vibration modes of H-OH bonds are revealed. The RE ions embedded in the phosphate network, acting as vitreous network modifiers, generate a depolymerization of the metaphosphate chains and an increasing of the non-bridging oxygen atoms number. The FTIR band specific to $(PO_3)^{2-}$ units from 1085 cm^{-1} in the case of Dy-doped glass is more pronounced by comparison with the other glasses. This is possibly due to Dy^{3+} ions that favor the formation of P-O-P bonds (bridging oxygen atoms) composed of metaphosphate groups $(PO_3)^{2-}$ on account of O-P-O (non-bridging oxygen atoms), the effect of depolymerization of the phosphate chains being reduced as compared to the other RE ions. The lowest intensity is noticed in the case of Yb-Er-doped glass, possibly due to the increasing of the atomic mass and decreasing of the ionic radius in the series Eu-Dy-Er-Yb, which causes a significant change of the local symmetry. The FTIR band from 1247 cm^{-1} in the case of the un-doped glass is more intense than in the case of REPGs, being almost negligible in the case of Dy-doped glass. Hence, it is possible to ascertain that the vibration mode of O-P-O units (non-bridging oxygen atoms) is almost missing due to the reduced depolymerization effect of Dy^{3+} ions.

The optical phonons of the non-bridging oxygen atom linked by the vitreous modifier ions (Li^+, Ba^{2+}, Al^{3+}, and rare-earth ions) are not observed in FTIR spectra as they present vibration modes at wavenumbers lower than 400 cm^{-1}.

The FTIR spectra of the un-doped and REPGs, in the range 1500-3500 cm^{-1} are presented in Fig. 3c. All the absorption bands are assigned to stretching and bending vibration modes of O-H bonds as well as combined vibrations [50,52,53].

In Fig.4b it is noticed that the Raman peak from 336 cm^{-1} specific to the un-doped glass is shifted towards lower wavenumbers accompanied by the decreasing of its intensity in the series Eu, Dy,

Yb-Er, Er-doped glasses. Thus, the bending of the phosphate network is less intense with increasing of the RE ions mass and decreasing of their ionic radius in the up-mentioned series. The symmetrical stretching vibration modes of O-P-O units are shifted towards lower wavenumbers in the case of Er and Yb-Er-doped glasses compared to the other glasses, possible due to the change of the local symmetry caused by these heavy ions. The intense Raman bands from 1086 cm^{-1} specific to $(PO_3)^{2-}$ units and O-P-O Raman bands from 1352 and 1369 cm^{-1} in the case of Er and, respectively, Yb-Er-doped glasses certify the change of the local symmetry.

3.4. Photoluminescence

Photoluminescence spectra of Eu, Dy, Er, and Yb-Er-doped glasses are presented in Figs. 5a, b, c, and d, respectively. Different excitation wavelengths were used, corresponding to the absorption bands from UV-Vis domain, presented in Figs. 2b, c, and d. In the following, only the spectra containing the most intense emission bands of the REPGS and the corresponding excitation wavelengths are presented.

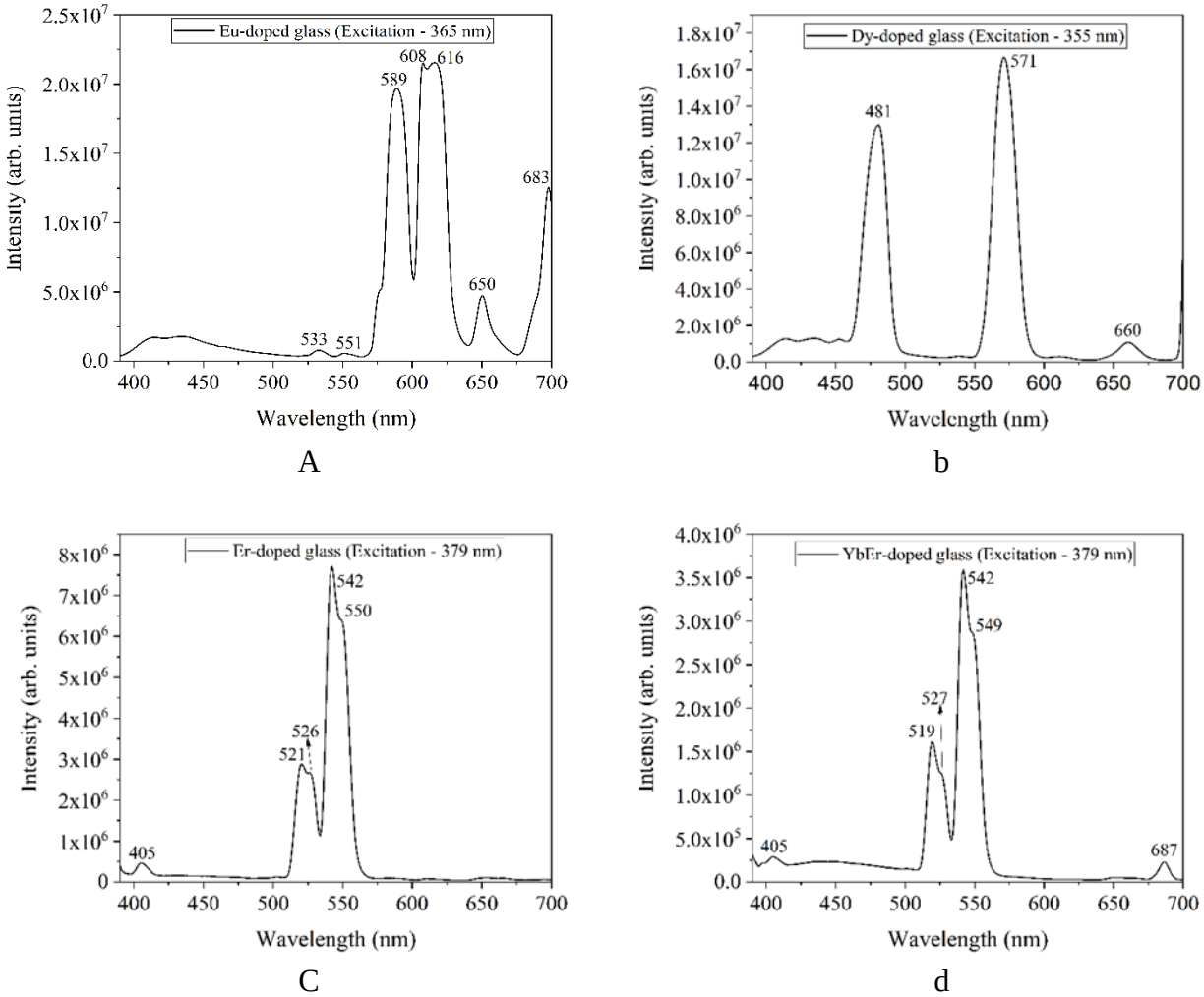

Fig. 5. Photoluminescence spectra of a) Eu; b) Dy; c) Er and d) Yb-Er-doped glasses.

The un-doped glass would certainly produce no photoluminescence in the UV-Vis domain as no absorption occurs as it results from Fig. 2a. Eu-doped glass exhibits visible emission bands by365 nm excitation (Fig.5a), the peaks are situated at 534, 552, 589, 608, 616, 650 and 698 nm. These maxima correspond to the following transitions: $^5D_1 \rightarrow {}^7F_1$, $^5D_0 \rightarrow {}^7F_2$, $^5D_0 \rightarrow {}^7F_0$, $^5D_0 \rightarrow {}^7F_1$, $^5D_0 \rightarrow {}^7F_2$, $^5D_0 \rightarrow {}^7F_3$, $^5D_0 \rightarrow {}^7F_4$ [5,6,58].

In the case of Dy-doped glass (Fig. 5b), several emission peaks were found by 365 nm excitation. Thus, the peaks placed at 414, 434, 453, 481, 571, and 661 nm are assigned to the following optical

transitions: $^4F_{7/2}\rightarrow{}^6H_{15/2}$, $^4G_{11/2}\rightarrow{}^6H_{15/2}$, $^4I_{15/2}\rightarrow{}^6H_{15/2}$, $^4F_{9/2}\rightarrow{}^6H_{15/2}$, $^4F_{9/2}\rightarrow{}^6H_{13/2}$, and $^4F_{9/2}\rightarrow{}^6H_{11/2}$ [7,10,59].

Er-doped glass exhibits luminescence in the green domain of the visible spectrum, collected by 379 nm excitation (Fig. 5c). Thus, two emission bands are noticed in the visible domain, namely 521-526 nm, 542-550 nm, corresponding to the $^2H_{11/2}\rightarrow{}^4I_{15/2}$ and $^4S_{3/2}\rightarrow{}^4I_{15/2}$ transitions, respectively [59].

In the case of Yb-Er-doped glass, excited by 379 nm (Fig. 5d), the emission spectrum presents only bands specific to Er^{3+} ions, 519-527 nm and 542-549 nm corresponding to $^2H_{11/2}\rightarrow{}^4I_{15/2}$ and $^4S_{3/2}\rightarrow{}^4I_{15/2}$ transitions, respectively. Yb^{3+} ions do not exhibit absorption bands in the UV-Vis domain except the band at 980 nm, corresponding to the transition $^2F_{7/2}\rightarrow{}^2F_{5/2}$ [59]. So, in the case of Yb-Er-doped glass, the green emission intensity is reduced in comparison with Er-doped glass emission, due to the low amount of Er_2O_3, 0.5 mol. % in the co-doped glass. The most intense emission band is noticed at 616 nm in the case of Eu-doped glass, followed by the peak at 571 nm in the case of Dy-doped glass and the less intense peak at 542 nm observed in both Er and Yb-Er-doped glasses.

In Fig. 6 is presented the experimental set-up for luminescence measurements in the temperature range ~(25-~-160^{o}C) using optical fibers (see Materials and Methods section). The glass sample was positioned on the heater plate and the bifurcated optical fiber as well as the thermocouple were situated on the sample surface. The thermocouple is connected to a multimeter, which displays permanently the temperature from the glass surface. The bifurcated fiber was used both to excite the glass sample from a light source (laser diode) and to collect the emission light.

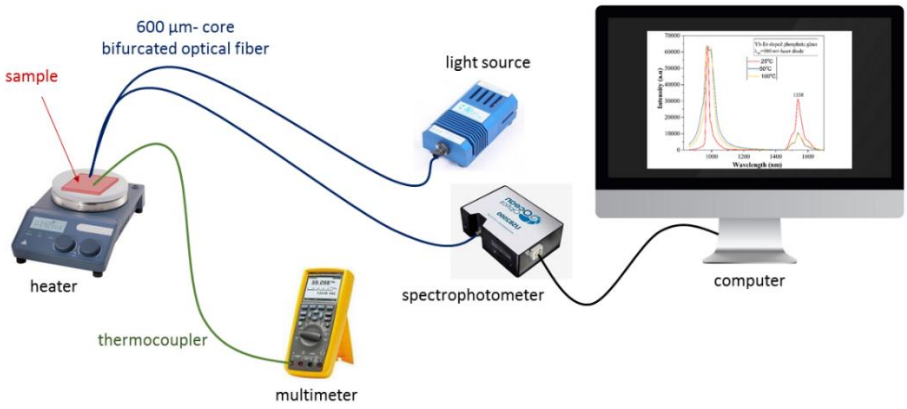

Fig.6. Experimental set-up used to measure the luminescence at room temperature as well as in the range ~(25-~160^{o}C).

In Figs. 7a and b, the emission spectra of Eu and, respectively, Dy-doped glasses, collected by 365 nm excitation, in the range ~(25-~160^{o}C), using optical fibers, are presented. The highest intensity peaks are noticed at 613 nm in the case of Eu-doped glass and, respectively, at 572 nm in the case of Dy-doped glass. In both cases, a relatively small decrease of the emission intensity with temperature is observed.

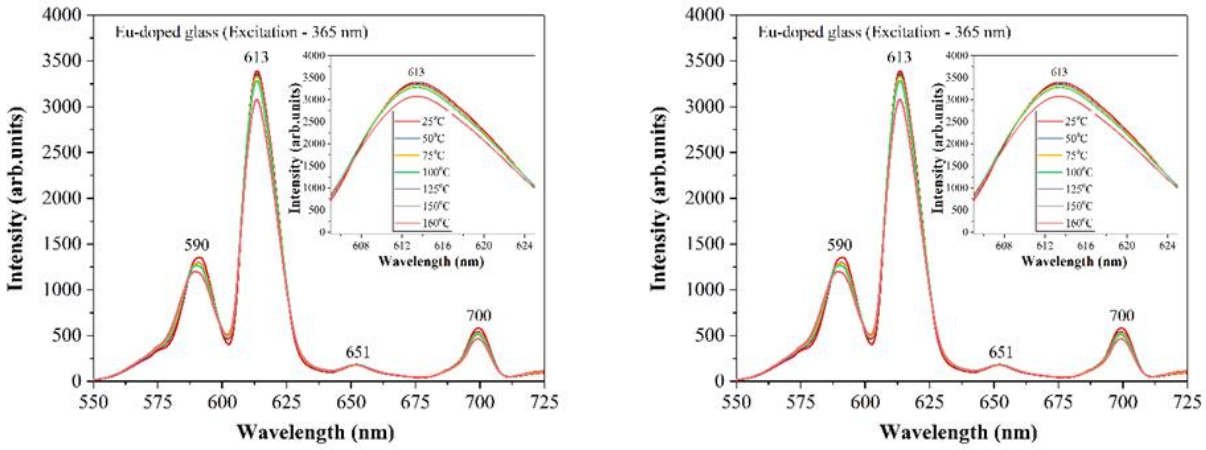

A b

Fig.7. Luminescence spectra of a) Eu and b) Dy-doped glasses, collected in the temperature range ~(25-~160°C).

In Figs. 8a and b, the emission spectra of Er and, respectively, Yb-Er-doped glasses, collected by 980 nm excitation, in the range ~(25-~160°C), using optical fibers, are presented. In both cases, the most intense peaks are found at 1538 nm and a decrease of the emission intensity was detected with temperature, being more important in the range ~(25-~100°C) in the case of Er-doped glass and ~(25-~125°C) in the case of Yb-Er-doped glass. .

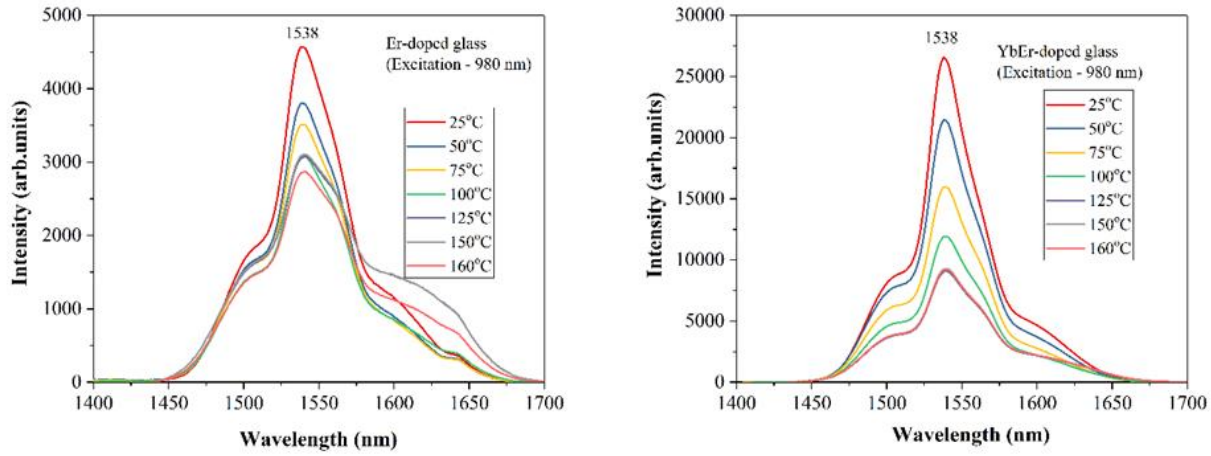

a b

Fig.8. Luminescence spectra of a) Er and b) Yb-Er-doped glasses, collected in the temperature range ~(25-~160°C).

Thus, Er^{3+} ions are excited from $^4I_{15/2}$ to $^4I_{11/2}$ level, then the ions pass by non-radiative relaxation to $^4I_{13/2}$ and, further on to the ground state by 1538 nm emission [59]. Yb-Er-doped glass was also excited by 980 nm laser diode in the temperature range ~(25-~160°C) and a relative intense emission band was noticed at 1538 nm [59]. The increase of the emission intensity in the case of Yb-Er-doped glass is due to the energy transfer from Yb^{3+} to Er^{3+} ions, ytterbium ions being excited from the ground state $^2F_{7/2}$ to the upper $^2F_{5/2}$ level, the latter corresponding to $^4I_{11/2}$ excited level of Er^{3+} ions. After the energy transfer, due to a larger absorbance cross-section of Yb^{3+} ions as compared to Er^{3+} ions, Er^{3+} ions are excited from $^4I_{11/2}$ to upper energy levels followed by non-radiative relaxation to $^4I_{13/2}$ and from this level to the ground state $^4I_{15/2}$, by radiative emission at 1538 nm. At the same time, by energy transfer from Yb^{3+} ions to Er^{3+} ions, an increased number of Er^{3+} ions are excited from the ground state $^4I_{15/2}$ to the excited level $^4I_{11/2}$, then by non-radiative relaxation the ions pass to $^4I_{13/2}$ and,

from here to the ground state by 1538 nm emission [42,59,60]. Briefly, the most intense emission peak is noticed at 1538 nm, in the case of Yb-Er-doped glass followed by the peak at 1538 nm in the case of Er-doped glass, a less intense peak of Eu-doped glass from 613 nm and the peak from 572 nm in the case of Dy-doped glass.

In Figs.9 a and b, the dependence of the emission peaks intensity of Eu and Dy-doped glasses with temperature is presented.

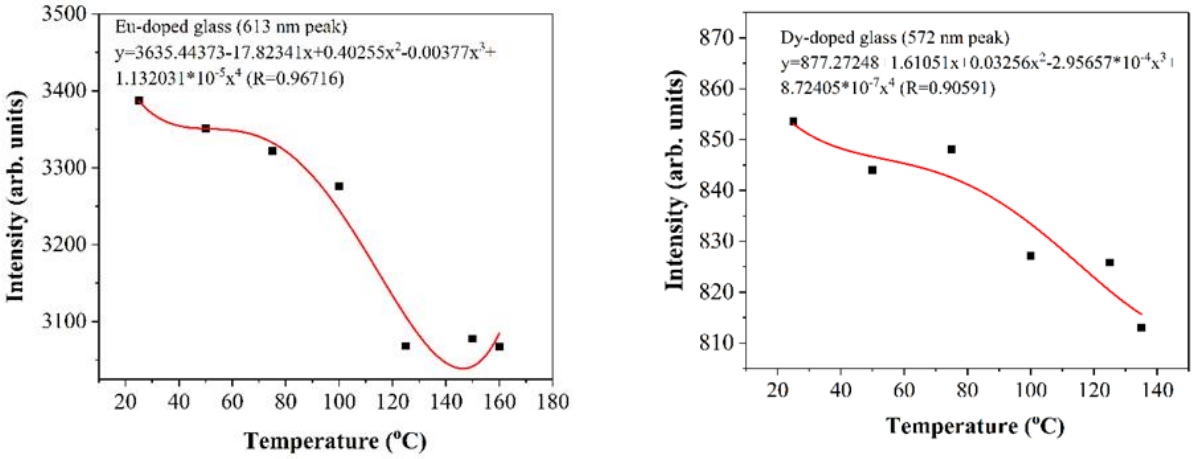

a b

Fig.9. Luminescence intensity versus temperature for a) Eu (613 nm) and b) Dy (572 nm)-doped glasses.

An approximate polynomial decrease of the luminescence intensity at 613 nm and 572 nm is taken into consideration in the case of Eu and, respectively, Dy-doped glass.

Figs.10 a and b, the dependence of the emission peaks intensity of Er and Yb-Er-doped glasses with temperature is presented. An approximate polynomial decrease of the luminescence intensity at 1538 nm is taken into account in the case of Er and, respectively, Er-Yb-doped glass. The correlation factors for all the fitted curves are indicated in the Figs. 9 and 10. A very accurate polynomial fitting is noticed in the case of Yb-Er-doped glass, the correlation factor being 1.

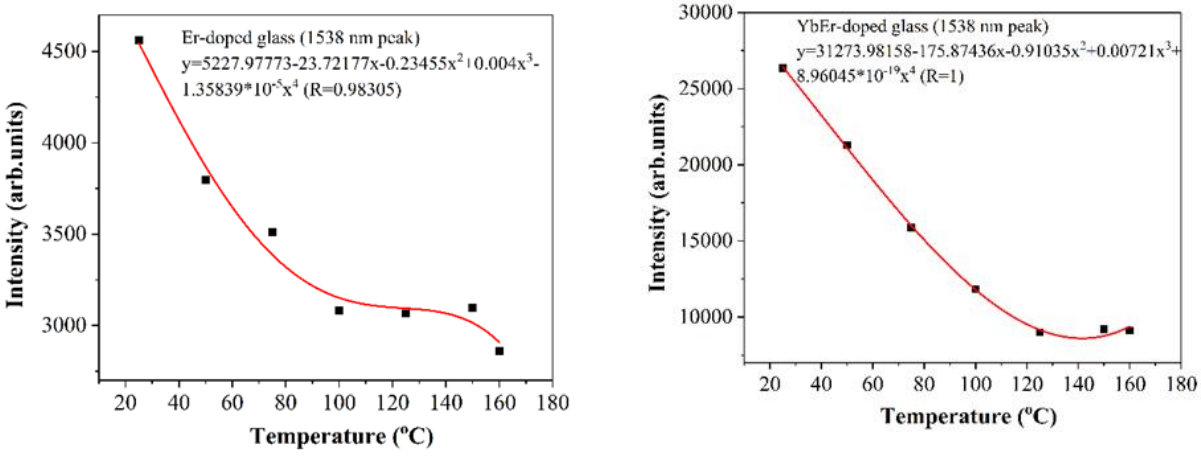

a b

Fig.10. Luminescence intensity versus temperature for a) Er (1538 nm) and b) Yb-Er (1538 nm)-doped glasses.

As seen from Fig.8b and 10b, Er-doped glass and, especially Yb-Er-doped glass are more sensitive to the temperature change as compared to the other rare-earth-doped glasses, which makes these co-doped materials potential candidates for sensing devices.

4. Conclusions

This study presents the synthesis, structural and optical characterization of the un-doped and Eu, Dy, Er, Yb-Er-doped glasses. Optical absorption in the case of REPGs shows bands characteristic to electronic f-f transitions, specific to each rare-earth dopant. FTIR and Raman spectroscopy evidenced some changes of the intensity and shifts of the respective bands in the case of REPGs compared to the un-doped glass. Eu and Dy-doped glasses show emission bands in the visible domain by UV excitation, at room temperature, corresponding to specific optical transitions of the doping ions. Er and Yb-Er-doped glasses exhibit a NIR emission band at room temperature by 980 nm excitation wavelength. In the case of Yb-Er-doped glasses, a considerable change of the luminescence intensity is noticed with temperature increase, by comparison with Eu and Dy-doped glasses. Therefore, Er and Yb-Er-doped glasses are promising materials for temperature sensing devices.

Acknowledgements

This work was supported by UEFISCDI (Executive Unity for Financing of Higher Education, Research and Innovation), Core Program, contracts no. 16N/2019, 18N/2019, and 21N/2019, project PN-III-P1-1.2-PCCDI-2017-0871/contract 47PCCDI/2018, project PN-III-P1-1.2-PCCDI-2017-0619/contract 42PCCDI/2018, by the Ministry of Research and Innovation through Program I - Development of the National R & D System, Subprogram 1.2 - Institutional Performance - Projects for Excellence Financing in RDI, contract no.19PFE/2018, and by Spanish State Research Agency and Spanish Ministry of Economy and Competitiveness through the project TEC2016-79367-C2-2-R.

References

[1] R.W. Tkach, Scaling optical communications for the next decade and beyond, Bell Labs Tech. J. 14(4) (2010) 3–9. https://doi.org/10.1002/bltj.20400.

[2] M. Klimczak, B. Siwicki, A. Heidt, R. Buczynski, Coherent supercontinuum generation in soft glass photonics crystal fiber, Photonics Res. 5(6) (2017) 710–727. https://doi.org/10.1364/PRJ.5.000710.

[3] A. de Pablos-Martin, M. Ferrari, M.J. Pascual, G.C. Righini, Glass-ceramics: a class of nanostructured materials for photonics, Riv. del Nuovo Cim. 38(7-8) (2015) 311–369. http://dx.doi.org/10.1393/ncr/i2015-10114-0.

[4] H. Bouchouicha, G. Panczer, D. de Ligny, Y. Guyot, R. Ternane, Luminescent properties of Eu-doped calcium aluminosilicate glass-ceramics: A potential tunable luminophore, Opt. Mat. 85 (2018) 41–47. https://doi.org/10.1016/j.optmat.2018.08.006.

[5] S. Rakpanich, N. Wantana, J. Kaewkhao, Development of bismuth borosilicate glass doped with Eu^{3+} for reddish orange emission materials application, Mater. Today: Proc. 4(5) Part 2 (2017) 6389–6396. https://doi.org/10.1016/j.matpr.2017.06.143.

[6] M. De, S. Sharma, S. Jana, Enhancement of $^5D_0 \rightarrow {}^7F_2$ red emission of Eu^{3+} incorporated in lead sodium phosphate glass matrix, Phys. B 556 (2019) 131–135. https://doi.org/10.1016/j.physb.2018.12.020.

[7] Y. Ye, S. Wang, H. An, 2019. White-light emission and chromaticity characterization of Dy^{3+} doped fluoride glass for standard white light source. J. of Non-Cryst. Solids 526, 119697. https://doi.org/10.1016/j.jnoncrysol.2019.119697.

[8] I. Kashif, H. Farouk, A. Ratep, M. Al Mahalawy, 2019. White light emission in Dy^{3+} doped $SiO_2B_2O_3Bi_2O_3TeO_2$ glass system. J. of Non-Cryst. Solids 522, 119581. https://doi.org/10.1016/j.jnoncrysol.2019.119581.

[9] S. Kaewjaeng, C. Jumpee, S. Kothan, J. Kaewkhao, N. Srisittipokakun, H. J. Kim, White emission from NaO-BaO-Bi_2O_3-SiO_2 glass system doped with Dy^{3+}, Mater. Today: Proc. 17 Part 4 (2019) 1774–1779. https://doi.org/10.1016/j.matpr.2019.06.210.

[10] K. Anilkumar, S. Damodaraiah, S. Babu, V. Reddy Prasad, Y.C. Ratnakaram, Emission spectra and energy transfer studies in Dy^{3+} and Dy^{3+}/Eu^{3+} co-doped potassium fluorophosphate glasses for white light applications, J. Lumin. 205 (2019) 190–196. https://doi.org/10.1016/j.jlumin.2018.09.007.
[11] H.K. Dan, D. Zhou, Z. Yang, Z. Song, X. Yu, J. Qiu, Optimizing Nd/Er ratio for enhancement of broadband near-infrared emission and energy transfer in the Er^{3+}–Nd^{3+} co-doped transparent silicate glass-ceramics, J. Non-Cryst. Solids 414 (2015) 21–26. http://dx.doi.org/10.1016/j.jnoncrysol.2015.02.001.
[12] Y. Xu, J. Qi, J. Ren, G. Chen, F. Huang, Y. Li, S. Lu, S. Dai, Luminescence and energy transfer in Er^{3+}/Nd^{3+} ion-codoped Ge–In–S–CsBr chalcohalide glasses, Mater. Res. Bull. 48(11) (2013) 4733–4737. https://doi.org/10.1016/j.materresbull.2013.08.015.
[13] K. Vemasevana Raju, C. Nageswara Raju, S. Sailaja, B. Sudhakar Reddy, Judd–Ofelt analysis and photoluminescence properties of RE^{3+} (RE=Er & Nd): Cadmium lithium boro tellurite glasses, Solid State Sci.15 (2013) 102–109. https://doi.org/10.1016/j.solidstatesciences.2012.08.011.
[14] B. Burtan, Z. Mazurak, J. Cisowski, M. Czaja, R. Lisiecki, W. Ryba-Romanowski, M. Reben, J. Wasylak, Optical properties of Nd^{3+} and Er^{3+} ions in TeO_2–WO_3– PbO–La_2O_3 glasses, Opt. Mater. 34 (12) (2012) 2050–2054. https://doi.org/10.1016/j.optmat.2012.03.030.
[15] G. Bai, L. Tao, K. Li, L. Hu, Y.H. Tsang, Enhanced light emission near 2.7 μm from Er–Nd co-doped germanate glass, Opt. Mater. 35(6) (2013) 1247–1250. https://doi.org/10.1016/j.optmat.2013.01.017.
[16] C.R. Kesavulu, H.J. Kim, S.W. Lee, J. Kaewkhao, N. Wantana, S. Kothan, S. Kaewjaeng, Influence of Er^{3+} ion concentration on optical and photoluminescence properties of Er^{3+}-doped gadolinium-calcium silica borate glasses, J. Alloy. Compd. 683 (2016) 590–598. https://doi.org/10.1016/j.jallcom.2016.04.314.
[17] P. Yu, L. Su, W. Guo, J. Xu, Photoluminescence and energy transfer progress in Er-doped Bi_2O_3-GeO_2 glasses, J. Lumin. 187 (2017)121–125. https://doi.org/10.1016/j.jlumin.2017.03.007.
[18] A. Madhu, B. Eraiah, P. Manasa, Ch. Basavapoornima, Er^{3+}-ions doped lithium-bismuth-boro-phosphate glass for 1532 nm emission and efficient red emission up conversion for telecommunication and lasing applications, J. of Non-Cryst. Solids 495 (2018) 35–46. https://doi.org/10.1016/j.jnoncrysol.2018.04.060.
[19] E. Cervantes-Juárez, A. N. Meza-Rocha, W. Romero-Romo, U. Caldiño, C. Falcony, E. Álvarez, M. Palomino-Ovando, R. Lozada-Morales, Up and down-shifting emission properties of novel Er^{3+}-doped CdO-V_2O_5-P_2O_5 glass system, Ceram. Int. 45(2) Part A (2019) 1609–1615. https://doi.org/10.1016/j.ceramint.2018.10.036.
[20] M. Li, J. Luan, Y. Zhang, F. Jiang, X. Zhou, J. Tang, K. Wang, Spectroscopic properties of Er/Yb co-doped glass ceramics containing nanocrystalline $Bi_2ZnB_2O_7$ for broadband near-infrared emission, Ceram. Int. 45(15) (2019) 18831–18837. https://doi.org/10.1016/j.ceramint.2019.06.116.
[21] Y. Liu, F. Song, G. Jia, Y. Zhang, Y. Tang, Strong emission in Yb^{3+}/Er^{3+} co-doped phosphate glass ceramics, Results Phys. 7 (2017) 1987–1992. https://doi.org/10.1016/j.rinp.2017.06.023.
[22] L.M. Marcondes, R.O. Evangelista, R.R. Gonçalves, A.S.S. de Camargo, D. Manzani, M. Nalin, F.C. Cassanjes, G.Y. Poirier, 2019. Er^{3+}-doped niobium alkali germanate glasses and glass-ceramics: NIR and visible luminescence properties. J. of Non-Cryst. Solids 521, 119492. https://doi.org/10.1016/j.jnoncrysol.2019.119492.
[23] H.K. Dan, N.L. Thai, L.D. Tin, J. Qiu, D. Zhou, Q. Jiao, Enhanced near/mid-infrared emission bands centered at ~1.54 and ~2.73 μm of Er^{3+}-doped in transparent silicate glass-ceramics via Mn^{2+}–Yb^{3+} dimer, Infrared Phys. Technol. 95 (2018) 33–38. https://doi.org/10.1016/j.infrared.2018.10.009.
[24] C. Nico, R. Fernandes, M.P.F. Graça, M. Elisa, B.A. Sava, R.C.C. Monteiro, L. Rino, T. Monteiro, Eu^{3+} luminescence in aluminophosphate glasses, J. Lumin. 145 (2015) 582-587. https://doi.org/10.1016/j.jlumin.2013.08.041.
[25] M. Elisa, B.A. Sava, I.C. Vasiliu, R.C.C. Monteiro, J.P. Veiga, L. Ghervase, I. Feraru, R. Iordanescu, Optical and structural characterization of samarium and europium-doped phosphate glasses, J. Non-Cryst. Solids 369 (2013) 55–60. https://doi.org/10.1016/j.jnoncrysol.2013.03.024.

[26] M. Elisa, B.A. Sava, I.C. Vasiliu, R.C.C. Monteiro, C.R. Iordanescu, I. Feraru, L. Ghervase, C. Tanaselia, M. Senila, B. Abraham, 2013. Investigations on optical, structural and thermal properties of phosphate glasses containing terbium ions, IOP Conf. Ser.: Mater. Sci. Eng. 47, 012025. https://doi.org/10.1088/1757-899X/47/1/012025.
[27] M. Elisa, B.A. Sava, I.C. Vasiliu, E.M. Carstea, I. Feraru, C. Tanaselia, M. Senila, B. Abraham, Optical and structural characterization of Eu^{3+}, Dy^{3+}, Ho^{3+} and Tm^{3+} -doped phosphate glasses, Phys. Chem. Glasses: Eur. J. Glass Sci. Technol. B, 53(5) (2012) 219-224.
[28] M. Elisa, I.C. Vasiliu, C.E.A. Grigorescu, B. Grigoraş, H. Niciu, D. Niciu, A. Meghea, N. Iftimie, M. Giurginca, R. Pătraşcu, J. Trodahl, M. Dalley, Characterization of aluminophosphate glasses containing Pr^{3+}, Er^{3+}, Gd^{3+} and Yb^{3+} ions, Adv. Mater. Res., 39-40 (2008) 61-64. https://doi.org/10.4028/www.scientific.net/AMR.39-40.61.
[29] S. Selvi, G. Venkataiah, S. Arunkumar, G. Muralidharan, K. Marimuthu, Structural and luminescence studies on Dy^{3+} doped lead boro–telluro-phosphate glasses, Phys. B 454 (2014) 72–81, http://dx.doi.org/10.1016/j.physb.2014.07.018.
[30] X-d. Wang, O.S. Wolfbeis, R.J. Meier, Luminescent probes and sensors for temperature, Chem. Soc. Rev. 42 (2013) 7834-7869, https://doi.org/10.1039/C3CS60102A.
[31] D. Chen, M. Xu, S Liu, X. Li, Eu^{2+}/Eu^{3+} dual-emitting glass ceramic for self-calibrated optical thermometry, Sens. Actuat. B 246 (2017) 756–760, http://dx.doi.org/10.1016/j.snb.2017.02.159.
[32] X. Li, Y. Yu, J. Hong, Z. Feng, X. Guan, D. Chen, Z. Zheng, Optical temperature sensing of Eu^{3+}-doped oxyhalide glasses containing $CsPbBr_3$ perovskite quantum dots, J. Lumin. 219 (2020) 116897, https://doi.org/10.1016/j.jlumin.2019.116897.
[33] Y. Chen, G.H. Chen, X.Y. Liu, T. Yang, Enhanced Up-Conversion Luminescence and Optical Thermometry Characteristics of Er^{3+}/Yb^{3+} Co-Doped Transparent Phosphate Glass-Ceramics, J. Lumin. 195 (2018) 314–320. https://doi.org/10.1016/j.jlumin.2017.11.049.
[34] J. Tang, Y. Huang, M. Sun, J. Gou, Y. Zhang, G. Li, Y.C Kang, J. Yang, Z. Xiao, Spectroscopic Characterization and Temperature-Dependent Upconversion Behavior of Er^{3+} and Yb^{3+} Co-Doped Zinc Phosphate Glass, J. Lumin. 197 (2018) 153–158. https://doi.org/10.1016/j.jlumin.2018.01.029.
[35] Y. Chen, X.Y. Liu, G.H. Chen, T. Yang, C.L. Yuan, C.R. Zhou, J.W. Xu, Up-conversion luminescence and temperature sensing characteristics of Er^{3+}/Yb^{3+} co-doped phosphate glasses, J Mater Sci: Mater Electron 28 (2017) 15657–15662. DOI 10.1007/s10854-017-7454-9.
[36] M. Elisa, R. Stefan, I.C. Vasiliu, M.I. Rusu, B.A. Sava, L. Boroica, M. Sofronie, V. Kuncser, A.C. Galca, A. Beldiceanu, A. Volceanov, M. Eftimie, 2019. Thermal, structural, magnetic and magneto-optical peculiarities of dysprosium-doped phosphate glass, J. Non-Cryst. Solids, 521, 119545. https://doi.org/10.1016/j.jnoncrysol.2019.119545.
[37] B.A. Sava, M. Elisa, L. Boroica, R.C.C. Monteiro, Preparation method and thermal properties of samarium and europium-doped alumino-phosphate glasses, Mater. Sci. Eng., B 178(20) (2013) 1429–1435. https://doi.org/10.1016/j.mseb.2013.09.001.
[38] M. Elisa, R. Iordanescu, C. Vasiliu, B.A. Sava, L. Boroica, M. Valeanu, V. Kuncser, A.C. Galca, A. Volceanov, M. Eftimie, A. Melinescu, A. Beldiceanu, Magnetic and magneto-optical properties of Bi and Pb-containing aluminophosphate glass, J. Non-Cryst. Solids 465 (2017) 55-58. https://doi.org/10.1016/j.jnoncrysol.2016.11.010.
[39] B.A Sava., L. Boroica, M. Elisa, Synthesis of rare-earth-doped phosphate glasses with improved optical properties, Rev. Rom. Mater. 43(3) (2013) 339-346.
[40] M. Elisa, B. A. Sava, L. Boroica, R. Iordanescu, I. Feraru, M. Eftimie, A. Beldiceanu, Aluminophosphate glasses containing rare-earth ions, used as optical sensors and the process for their obtaining them, Patent no. 130686/30.07.2019.
[41] G. Gouadec, P. Colomban, Raman Spectroscopy of nanomaterials: How spectra relate to disorder, particle size and mechanical properties, Prog. Cryst. Growth Ch. 53(1) (2007) 1-56. https://doi.org/10.1016/j.pcrysgrow.2007.01.001.

[42] S. Tabanli, G. Eryurek, Optical investigation of Er^{3+} and Er^{3+}/Yb^{3+} doped zinc-tellurite glass for solid-state lighting and optical thermometry, Sens. Actuators, A 285 (2019) 448–455. https://doi.org/10.1016/j.sna.2018.11.043.
[43] M. Pokhrel, G.A. Kumar, S. Balaji, R. Debnath, D.K. Sardar, Optical characterization of Er3+and Yb3+ co-doped barium fluorotellurite glass, J. Lumin. 132(8) (2012) 1910–1916. https://doi.org/10.1016/j.jlumin.2012.02.041.
[44] M. Li, J. Luan, Y. Zhang, F. Jiang, X. Zhou, J. Tang, K. Wang, Spectroscopic properties of Er/Yb co-doped glass ceramics containing nanocrystalline $Bi_2ZnB_2O_7$ for broadband near-infrared emission, Ceram. Int. 45(15) (2019) 18831–18837. https://doi.org/10.1016/j.ceramint.2019.06.116.
[45] Y.M. Lai, X.F. Liang, S.Y. Yang, J.X. Wang, L.H. Cao, B. Dai, Raman and FTIR spectra of iron phosphate glasses containing cerium, J. Mol. Struct. 992(1-3) (2011) 84–88. https://doi.org/10.1016/j.molstruc.2011.02.049.
[46] G.E. Stan, A.C. Popa, A.C. Galca, G. Aldica, J.M.F. Ferreira, Strong bonding between sputtered bioglass–ceramic films and Ti-substrate implants induced by atomic inter-diffusion post-deposition heat-treatments, Appl. Surf. Sci. 280 (2013) 530–538. https://doi.org/10.1016/j.apsusc.2013.05.022.
[47] R.K. Brow, R.J. Kirkpatrick, G.L. Turner, Local structure of $xAl_2O_3 \cdot (1-x)NaPO_3$ Glasses: An NMR and XPS study, J. Am. Ceram. Soc. 73(8) (1990) 2293-2300. https://doi.org/10.1111/j.1151-2916.1990.tb07591.x.
[48] P.K. Jha, O.P. Pandey, K. Singh, FTIR spectral analysis and mechanical properties of sodium phosphate glass–ceramics, J. Mol. Struct. 1083 (2015) 278–285, https://doi.org/10.1016/j.molstruc.2014.11.027.
[49] A.C. Popa, G.E. Stan, M.A. Husanu, I Mercioniu, L.F. Santos, H.R. Fernandes, J.M.F. Ferreira, Bioglass implant-coating interactions in synthetic physiological fluids with varying degrees of biomimicry, Int. J. Nanomed. 12 (2017) 683–707. https://doi.org/10.2147/IJN.S123236.
[50] S.-P. Tung, B.-J. Hwang, High proton conductive glass electrolyte synthesized by an accelerated sol–gel process with water/vapor management, J. Membr. Sci. 241(2) (2004) 315-323. https://doi.org/10.1016/j.memsci.2004.06.003.
[51] D. Muresan, M. Dragan Bularda, C. Popa, L. Baia, S. Simon, Structural and biological investigations of phosphate glasses with silver, Rom. J. Phys. 51(1–2) (2006) 231–237.
[52] Y.S. Kim, R.E. Tressler, Microstructural evolution of sol-gel-derived phosphosilicate gel with heat treatment, J. Mater. Sci. 29 (1994) 2351-2535. https://doi.org/10.1007/BF00363451.
[53] S. Talam, R. Busi, N. Gunnam, P.S. Prasad, V.R. Penugonda, Preparation and structural characterization of P_2O_5-CaO-Na_2O:CuO glasses, J. Optoelectron. Adv. M. 21(7-8) (2019) 530-535.
[54] J. Diao, X. Xu, D. Zhang, T. Zheng, Z. Li, J. Lv, Effect of SnO addition on structure and properties of P_2O_5-SnF_2-WO_3-B_2O_3 glasses for low temperature sealing, Optoelectron. Adv. Mat. 13(11-12) (2019) 613-619.
[55] C. Dayanand, G. Bhikshamaiah, V. Jaya Tyagaraju, M. Salagram, A.S.R. Krishna Murthy, Structural investigations of phosphate glasses: a detailed infrared study of the x(PbO)-(1−x) P_2O_5 vitreous system, J. Mater. Sci. 31 (1996) 1945-1967. https://doi.org/10.1007/BF00356615.
[56] K.J. Rao, K.C. Sobha, S. Kumar, Infrared and Raman spectroscopic studies of glasses with NASICON-type chemistry, J. Chem. Sci. 113 (2001) 497-514. https://doi.org/10.1007/BF02708786.
[57] J.J. Hudgens, R.K. Brow, D.R. Tallant, S.W. Martin, Raman spectroscopy of the structure of lithium and sodium ultraphosphate glasses, J. Non-Cryst. Solids 223(1-2) (1998) 21-31. https://doi.org/10.1016/S0022-3093(97)00347-5.
[58] Q. Wei, C. ma, M. Zhao, G. Ren, C. Su, Preparation and optical properties of Na^+/Eu^{3+} Co-doped CaO-WO_3-SiO_2 transparent glass-ceramics, J. Optoelectron. Adv. M. 22(3-4) (2020) 182-186.
[59] X. Wang, Q. Liu, Y. Bu, C.-S. Liu, T. Liu, X. Yan, Optical temperature sensing of rare-earth ion doped phosphors, RSC Adv. 5 (2015) 86219- 86236. https://doi.org/10.1039/C5RA16986K.
[60] Y. Zhang, M. Li, J. Li, J. Tang, W. Cao, Z. Wu, Optical properties of Er^{3+}/Yb^{3+} co-doped phosphate glass system for NIR lasers and fiber amplifiers, Ceram. Int. 44(18) (2018) 22467–22472. https://doi.org/10.1016/j.ceramint.2018.09.015.

Table captions

Table 1. Molar composition of rare-earth-doped phosphate glasses.

Table 2. Assignment of FTIR and Raman bands for REPGs.

Figure captions

Fig. 1. XRD patterns of un-doped glass, Eu, Er, Dy, and Yb-Er-doped glasses, respectively.

Fig. 2. Optical absorption of a) un-doped; b) Eu; c) Dy and d) Er and Yb-Er doped glasses, respectively.

Fig. 3. FTIR spectra of a) un-doped glass in the range 450-1500 cm^{-1}; b) REPGs in the range 450-1500 cm^{-1}; c) REPGs in the range 1500-3500 cm^{-1}.

Fig.4. Raman spectra of a) the un-doped glass; b) REPGS

Fig. 5. Photoluminescence spectra of a) Eu; b) Dy; c) Er and d) Yb-Er-doped glasses.

Fig.6. Experimental set-up used to measure the luminescence at room temperature as well as in the range ~(25-~160^{o}C).

Fig.7. Luminescence spectra of a) Eu and b) Dy-doped glasses, collected in the temperature range ~(25-~160^{o}C).

Fig.8. Luminescence spectra of a) Er and b) Yb-Er-doped glasses, collected in the temperature range ~(25-~160^{o}C).

Fig.9. Luminescence intensity versus temperature for a) Eu (613 nm) and b) Dy (572 nm)-doped glasses.

Fig.10. Luminescence intensity versus temperature for a) Er (1538 nm) and b) Yb-Er (1538 nm)-doped glasses.